Diffusion Kurtosis Imaging of the neonatal Spinal Cord: design and application of the first processing pipeline implemented in Spinal Cord Toolbox

Rosella Trò[1*], Monica Roascio[1], Domenico Tortora[2], Mariasavina Severino[2], Andrea Rossi[2,3], Julien Cohen-Adad[4,5,6], Marco Massimo Fato[1], Gabriele Arnulfo[1,7]

From the [1]Department of Informatics, Bioengineering, Robotics and System Engineering (DIBRIS), University of Genoa, Genoa, Italy; [2]Neuroradiology Unit, Istituto Giannina Gaslini, Genoa, Italy; [3]Department of Health Sciences (DISSAL), University of Genoa, Genoa, Italy; [4]NeuroPoly Lab, Institute of Biomedical Engineering, Polytechnique Montreal, Montreal, QC, Canada; [5]Functional Neuroimaging Unit, CRIUGM, Université de Montréal, Montreal, QC, Canada; [6]Mila - Quebec AI Institute, Montreal, QC, Canada; [7]Neuroscience Center, Helsinki Institute of Life Science, University of Helsinki, Helsinki, Finland

*Corresponding author. Department of Informatics, Bioengineering, Robotics and System Engineering (DIBRIS), University of Genoa, Via all'Opera Pia, 13, 16145 Genoa, Italy, rosella.tro@edu.unige.it

Abstract

Diffusion Kurtosis Imaging (DKI) has undisputed advantages over more classical diffusion Magnetic Resonance Imaging (dMRI), as witnessed by a fast-increasing number of clinical applications and software packages widely adopted in brain imaging domain. Despite its power in probing tissue microstructure compared to conventional MRI, DKI is still largely underutilized in Spinal Cord (SC) imaging because of its inherently demanding technological requirements.

If state-of-the-art hardware advancements have recently allowed to make great strides in applying this emerging method to adult and child SC, the same does not apply to neonatal setting. Indeed, amplified technical issues related to SC district in this age range have made this field still unexplored. However, results arising from recent application of DKI to adult and child SC are promising enough to suggest how informative this technique would be in investigating newborns, too.

Due to its extreme sensitivity to non-gaussian diffusion, DKI proves particularly suitable for detecting complex, subtle, fast microstructural changes occurring in this area at this early and critical stage of development, and not identifiable with only DTI. Given the multiplicity of congenital anomalies of the spinal canal, their crucial effect on later developmental outcome, and the close interconnection between SC region and the above brain, managing to apply such a method to neonatal cohort becomes of utmost importance.

In this work, we illustrate the first semi-automated pipeline for handling with DKI data of neonatal SC, from acquisition setting to estimation of diffusion (DTI & DKI) measures, through accurate adjustment of processing algorithms customized for adult SC. Each processing step of this pipeline, built on Spinal Cord Toolbox (SCT) software, has undergone Quality Control check by supervision of an expert pediatric neuroradiologist, and the overall procedure has preliminarily been tested in a pilot clinical case study. Results of this application agree with findings achieved in a corresponding adult survey, thus confirming validity of adopted pipeline and diagnostic value of DKI in pediatrics. This novel tool hence paves the wave for extending its application also to other promising advanced dMRI models, such as Neurite Orientation Dispersion and Density Imaging (NODDI), and to a wider range of potential clinical applications concerning neonatal period.

Keywords

Spinal Cord, DTI, DKI, processing pipeline, pediatric imaging

1. Introduction

In recent years, an increasing number of works in the field of neuroimaging are stressing the importance to move beyond simplistic assumptions of Diffusion Tensor Imaging (DTI) model (Tournier, 2019) towards more advanced diffusion MRI (dMRI) methods, among which DKI (Jensen et al., 2005) is one of the most promising (Farquharson et al., 2013; Loucao et al., 2015; Mader and Urbach, 2013).

Within existing non-standard techniques, DKI has indeed turned out to be especially suitable for imaging of SC, a structure where the assumption of Gaussian diffusion fails. Indeed, the presence of Gray Matter (GM) in the central portion contains a significant amount of cell membranes and organelles that limits diffusion to fewer directions. Taking into account pathological processes not

following a Gaussian distribution, DKI provides a better understanding of the underlying micromolecular environment. In fact, it exhibits increased sensitivity in microstructural assessment of both White Matter (WM) and GM (Wu and Cheung, 2010). Hence this susceptibility translates into an increased amount of diagnostic information, beyond that obtained with routine diffusion metrics.

Latest technological advances on reduced field-of-view techniques to mitigate susceptibility artifacts and cardiac/respiratory gating have allowed to overcome most of the methodological challenges inherent to adult SC imaging (Taber et al., 1998). Thanks to these strategies, DKI by now represents a promising tool for studying a plethora of spine disorders with minor modifications to protocol parameters in use for brain imaging (Bester et al., 2010, 2009; Li and Wang, 2017, 2015; Panara et al., 2017; Raz et al., 2013).

The scenario becomes definitely more complicated when attempting to translate this imaging technique to the pediatric clinical setting (Sorantin et al., 2008; Thukral, 2015). Along with typical issues inherent to SC district - small cross-sectional area requiring high spatial resolution; interface between regions with different magnetic properties; Partial Volume Effect (PVE) of pulsating Cerebro-Spinal Fluid (CSF) with each heartbeat; bulk physiologic motion due to proximity of heart and pulmonary parenchyma - further complications here arise from a multiplicity of factors related to the age range under analysis. Anatomic structures are even smaller in children; possibility of subject motion is increased, including also infant tongue's sucking motion; artifact-reducing techniques like cardiac gating and respiratory compensation as well as suppression sequences (Wilm et al., 2007) are often unfeasible since time-consuming; sedation is typically not desirable in children or neonates and risk of radiofrequency heating effects is higher due to smaller patient's size. All aforementioned issues result in artifact-laden, low-signal images, which are often suboptimal for diagnostic evaluation.

Adopted solutions for improving image resolution and reducing artifacts comprise induction of natural sleep without sedation (by feeding the patient immediately before MR examination) and the use of a vacuum fixation pillow to wrap the patient as well as of special ear muffs to protect from noise. However, the main requirement when handling with pediatric dMRI data is the choice of a proper acquisition protocol tailored for pediatric imaging, made up of low angular resolution, low b-values and few gradient directions, likewise in pediatric brain (Toselli et al., 2017). If for adult SC acquisition time is preferably reduced with respect to the brain, minimization of scan time is the only real solution to reduce the appearance of artifacts in pediatrics. Nevertheless, this forced time

minimization clashes with specific requirements of advanced diffusion methods in terms of acquisition sequences.

Indeed, contrary to DTI, higher-order diffusion models, including DKI, require multi-shell high angular resolution diffusion imaging (HARDI) sequences (Webster and Descoteaux, 2015), typically involving several high b-values distributed on a high number of gradient directions, grouped in shells. This implies longer acquisition times, straining the feasibility of advanced dMRI methods in pediatrics. Resorting to optimized acquisition sequences (Andre and Bammer, 2010), often combined with state-of-the-art techniques such as Parallel Imaging (Fruehwald-Pallamar et al., 2012) and Multi-Band, can significantly increase acquisition speed and reduce artifacts. However, these advanced technologies are not always available in a real clinical scenario due to high costs and technical limitations.

If extension of DTI to the pediatric SC has shown promising results in a wide range of clinical conditions, as evidenced by the increasing number of works on the topic (Alizadeh et al., 2018b, 2018a; Antherieu et al., 2019; Mohamed et al., 2011; Mulcahey et al., 2013; Reynolds et al., 2019; Saksena et al., 2018a, 2018b, 2016; Singhi et al., 2012), what immediately stands out while reviewing literature on pediatric SC is the absence of studies concerning DKI and particularly applied to the neonatal period (0-1 month).

To the best of our knowledge, the only published work on pediatric DKI (Conklin et al., 2016) is limited to grown-up children (6-16 years), whose larger anatomical structures and reduced source of movements enable better image quality and longer scan times. Indeed, in newborns, SC dimensions themselves (24 cm average length and 4.4 mm diameter, which can further decrease in case of malformations (Singh et al., 2020)), are enough to conceive amplification of aforementioned technical issues and thus justify the lack of research towards this direction.

However, the ability of DKI to offer additional and complementary information to DTI may bring a significant contribution in investigating such decisive and delicate stage of development, especially if we consider the wide range of developmental anomalies of the spinal canal affecting infants at birth (Kaplan et al., 2005; Oskouian et al., 2007; Rufener et al., 2011; S Basu et al., 2002).

In this paper, we introduce the first complete pipeline (from image acquisition to computation of diffusion metrics passing through SC motion correction, segmentation and registration with atlas) specifically designed for neonatal imaging and able to address all methodological issues posed by this age range. Applicability and clinical validity of proposed method has been evaluated analyzing a specific clinical case-study in collaboration with Neuroradiology Unit of Gaslini Children's Hospital.

2. Methods

2.1. Full pipeline description

Our pipeline integrates MRtrix3 (v.3.0.1) (Tournier et al., 2019) for setting of dMRI acquisition sequence, Spinal Cord Toolbox (SCT, v. 4.1.0, https://github.com/neuropoly/spinalcordtoolbox) (de Leener et al., 2017a) for all processing steps specific to the SC, and Diffusion Imaging in Python (Dipy, v.1.1.1) (Garyfallidis et al., 2014) for computation of diffusion metrics.

Output of key processes, such as segmentation and registration with atlas, can be checked through SCT Quality Control (QC) module, which automatically generates reports consisting in HTML files, containing a table of entries and allowing to show, for each entry, animated images (background with overlay on and off) for data quality validation.

In our methodological pipeline we have opted for mainly relying on SCT, being currently the only existing fully-comprehensive, free and open-source software dedicated to the processing and analysis of multi-parametric MRI of the spinal cord (Battiston et al., 2018; Brooks et al., 2017; Duval et al., 2017; Eippert et al., 2017; Kong et al., 2014; Ljungberg et al., 2017; Massire et al., 2016; Samson et al., 2016; Taso et al., 2016; Vahdat et al., 2015; Weber et al., 2018, 2016) successfully employed in a plethora of clinical applications concerning adult SC (Castellano et al., 2016; Grabher et al., 2016; Hori et al., 2018; Huber et al., 2018; Martin et al., 2017; McCoy et al., 2017; Smith et al., 2018; Talbott et al., 2016; Ventura et al., 2016; Yiannakas et al., 2016).

An overview of our image processing pipeline highlighting key features is shown in Figure 1. Since SCT algorithms are validated in adult imaging, we specifically customized each processing step to our neonatal scans. Our pipeline thus represents, to the best of our knowledge, the first semi-automated ad-hoc procedure for imaging of neonatal spine. A fully automatic workflow is not feasible here: acquisition time constraints, available scanner features and subsequent image quality require inevitable although minimal and highly reproducible manual interventions. A detailed description for each image processing step is reported in the sections below.

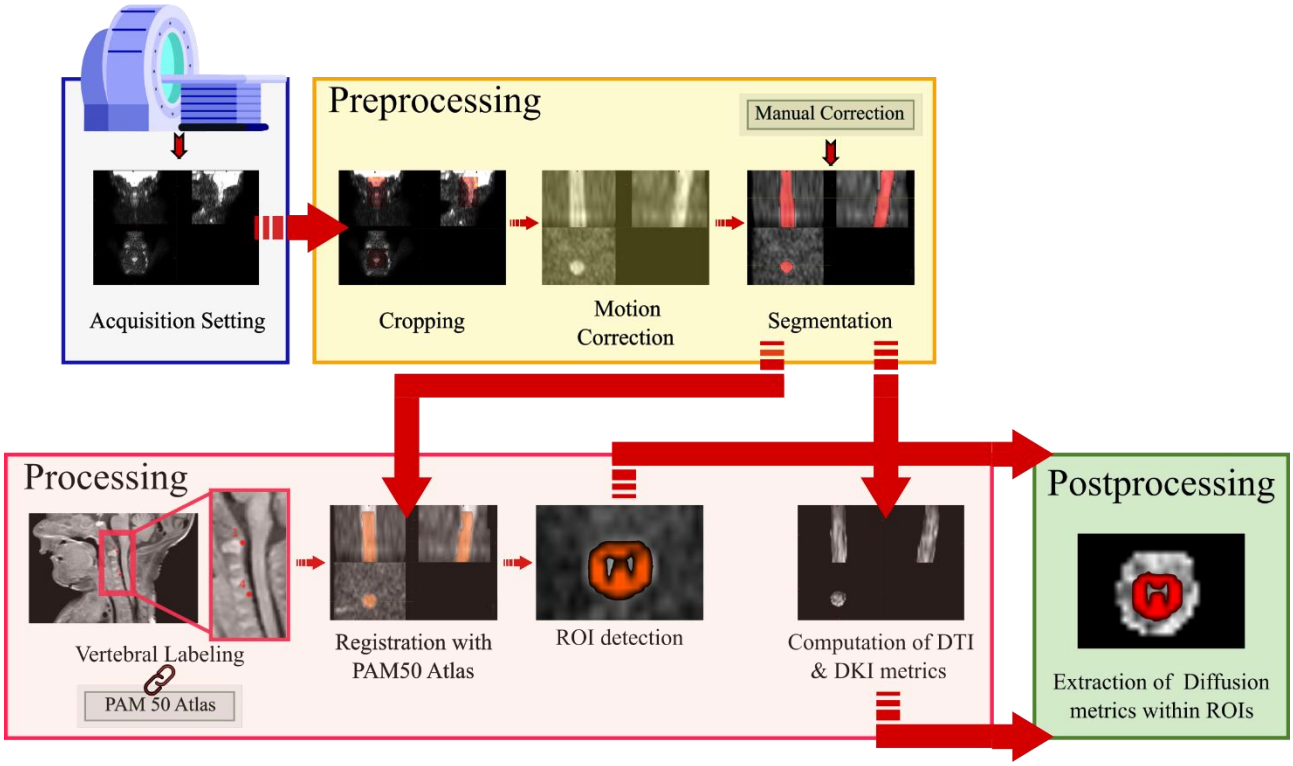

Figure 1. Overall Processing Pipeline: designed pipeline allows complete handling of DKI scan of neonatal Spinal Cord from acquisition setup to preprocessing, processing and postprocessing steps

2.2. Customized acquisition sequence

Given the lack of a specific acquisition protocol for DKI of neonatal SC, we designed the diffusion-weighting scheme in collaboration with the neuroradiologists at Gaslini Hospital. One constraint we had to deal with was the impossibility to perform optimized variants of Spin-Echo Echo Planar Imaging (SE-EPI) sequence (i.e. reduced FOV or spatially selective techniques) (Andre and Bammer, 2010) on Philips Ingenia scanner. Therefore, minimization of scan time was our main focus in order to suppress motion and fast CSF pulsation artifacts typical of newborns.

We thus tested different versions of diffusion-weighted gradient scheme, adopting optimal trade-off between Fiber Orientation Distributions profile (FODs, estimated with Mrtrix3 using Multi-Shell Multi-Tissue Constrained Spherical Deconvolution (MS-MT CSD)), image quality and scan time as a criterion for diffusion gradient scheme selection.

We generated each multi-shell diffusion gradient table through Mrtrix3 script *gen_scheme*, taking as inputs the number of phase-encoding directions to be included in the scheme (for most scanners,

including ours, typically 1), the b-value of the shell, and the number of directions to include in the shell. The procedure adopted in this script ensures uniform sampling by maximizing uniformity within shells using a bipolar electrostatic repulsion model for optimal angular coverage.

We first tried to directly apply the scheme already in use at the Neuroradiology Unit for infant brain, made up of 9 b=0; 45 b=700 and 45 b=2700 s/mm². However, this produced low-quality images, where signal and background noise were difficult to distinguish. In addition, b=0 images could not be discriminated from non b=0 volumes and it was really hard to detect anatomical SC details.

We thus conceived a second version consisting in a lower number of directions and reduced maximum b-value: 6 b=0; 30 b=700; and 24 b=2100 s/mm² with a scan time of 9 minutes. Anatomical features are here sharper and the image is overall less noisy.

Nevertheless, we opted for further reducing acquisition time without significantly affecting image quality.

We hence applied the MultiBand slice acceleration technique (Barth et al., 2016) (https://www.usa.philips.com/healthcare/resources/landing/compressed-sensecombined).

The final version of diffusion acquisition scheme is displayed in Figure 2 and includes 6 b=0; 13 b=700 and 13 b=2100 s/mm² for a duration of 4 minutes 30 s. This is the best possible solution that combines conflicting requirements of complex multi-shell acquisition and minimized scan time.

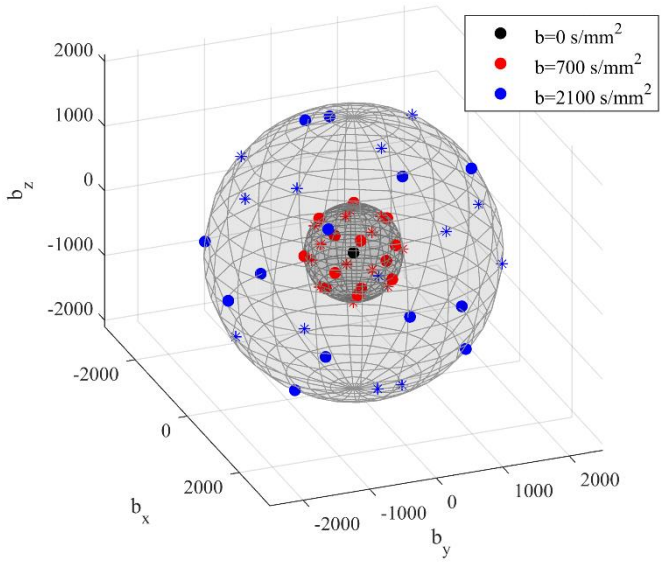

Figure 2. **3D view of final diffusion acquisition scheme:** directions of diffusion-sensitizing gradients relative to each b-value are displayed in three different colors as reported in the legend. Units are in s/mm^2. Opacity indicates polarity: opaque are the polarities in the set, transparent their opposite

Along with dMRI, we also acquired a structural image as anatomical reference. The definitive MRI protocol thus consisted in a Turbo Spin Echo (TSE) 3D T1-weighted image followed by a DKI series whose details are listed in Table 1.

	3dT1	**DKI**
TR/TE (s)	0.6/0.026337	3.378/0.128
Diffusion Scheme (s/mm²)	–	6 b=0, 13 b=700, 13 b=2100
Flip Angle (°)	90	90
Acquisition Matrix	251*512	160*160
Multi-Band Factor	–	2
Acquisition Resolution (mm)	0.50*0.38*0.38	0.8*0.8*4
Slice Thickness (mm)	0.38, 0.5 mm gap	4, without gap
Slice Orientation	–	axial
# Slices	512	24
Field of View (FOV) (mm)	195x195x126	128x93x96
Total Scan Time	4 minutes 5 s	4 minutes 30 s

Table 1: Data Acquisition Details for both structural 3D T1 and DKI image

2.3. Preprocessing

All steps concerning preprocessing phase are illustrated in detail below and summarized in Figure 3.

2.3.1. Cropping

SC scans usually include also cerebral areas such as medulla and cerebellum due to their proximity with cervical SC. In order to exclusively focus on the area of interest excluding undesired voxels, as a first preprocessing step, we thus recommend to apply to DKI images SCT function *sct_crop_image*

in order to fasten subsequent processing. FOV reduction thus allows to close out all non-spinal areas as well as spinal levels whose corresponding slices are not usable due to poor image quality (Figure 3a).

Lower and higher bounds for cropping along the three spatial coordinates can be specified via command line in order to select the same area of interest (i.e. cSC) for all the cohort, considering FOV positioning is consistent across subjects.

2.3.2. Motion Correction

Within-subject registration of SC data is a complex issue because of the articulated structure of the spine, which can produce non-rigid deformations. Therefore, in contrast to the brain, affine transformations included in standard motion-correction algorithms result inadequate in terms of accuracy and are set aside in favour of slice-wise translations in axial plane.

To this end, SCT features a complex motion correction framework *sct_dmri_moco* based on a combination of tools.

First of all, *SliceReg* algorithm estimates slice-by-slice translations while ensuring regularization constraints along z axis. The latter is achieved using a polynomial function (order specified by the user, flag *-param*). This method was shown to offer better accuracy and robustness than rigid-body transformations and non-regularized slice-by-slice registration, respectively (de Leener et al., 2017a).

Moreover, motion correction in SCT includes another feature first proposed in (Xu et al., 2013) to improve the robustness of registration in high b-value diffusion MRI data such as DKI datasets. It consists in grouping adjacent volumes and estimating the transformation relying on these successive subsets (typically from 3 to 5 volumes) averaged together (flag *-g*).

This robust slice- and group- wise motion correction is applied here with default parameters: grouping of 3 successive dMRI volumes, regularization with 2nd order polynomial function, unitary smoothing kernel (1 mm), Mutual Information (MI) as metric used for registration, and final spline interpolation (flag *-x*) (Figure 3b).

Since *sct_dmri_moco* works through iterative average over groups of successive slices in order to increase the SNR of the target image, its output includes a 3D volume corresponding to the mean from DKI slices. These motion-corrected average DKI data will serve as input for subsequent segmentation thanks to its excellent cord contrast.

2.3.3. Segmentation

Proper segmentation of SC is decisive for subsequent steps of template registration and computation of metrics along the cord.

Detection of SC has turned out to be a thorny step, since standard SCT algorithm *propseg*, based on multi-resolution propagation of tubular deformable models (de Leener et al., 2014), is trained for adult spine.

Given the reduced size of neonatal SC and the low contrast between the spine and CSF, default segmentation method fails in several slices even modulating the algorithm parameters - e.g. manual initialization of spinal cord centerline through interactive viewer (flag *-init-mask*), selection of SC radius size (flag *-radius*) or cord rescale (flag *-rescale*).

We thus resort to a more recent and advanced method of SC extraction, based on deep learning *sct_deepseg_sc* (Gros et al., 2019). This fully automatic segmentation framework was conceived for detecting SC and intramedullary MS lesions from a variety of MRI contrasts and resolutions.

It is composed of a cascade of two convolutional neural networks (CNN), specifically designed to deal with spinal cord morphometry: the first detects the cord centerline and reduces the space around the spinal cord (for better class balance), and the second segments the cord.

Segmentation results outperformed *sct_propseg*, showing higher robustness to variability in both image parameters and clinical conditions.

Thanks to its versatility, the application of this method results suitable also for neonatal imaging, allowing robust and accurate segmentation of our scans without ever the need of additional parameters but just specifying the kind of image contrast as *dwi* (flag *-c*) (Figure 3c).

In case of failure of SC detection (related to the onset of artifacts at acquisition phase and not to a flaw with the algorithm), we necessarily opt for manual correction of problematic slices on FSL editor (*FSLeyes*) (Figure 3d,e).

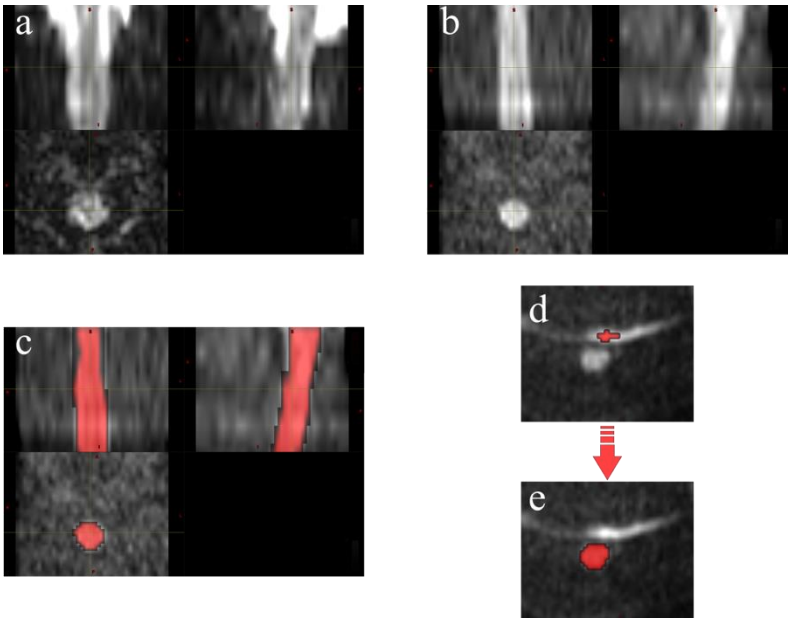

Figure 3. **Preprocessing:** DKI scan through preprocessing steps for one example subject: (a) FOV reduction; (b) Motion Correction; (c) Segmentation: Deep Learning Segmentation algorithm generally achieves satisfactory results in SC detection; (d) Example of artefactual slice due to a poor fat saturation, causing the fat to alias on the spinal cord area and (e) requiring manual correction of segmentation

2.4. Processing

2.4.1. Vertebral Labeling

After segmentation, labeling of vertebral levels or discs is the second mandatory step in order to match the template to the subject's MRI (template registration).

Two vertebral levels are necessary for registering data to the template. Each of these two landmarks consists of a voxel placed in the middle of the SC, at the level of the corresponding mid-vertebral body, and assigned a relative number starting from 1 for C1 vertebra. However, SCT recently introduced the possibility to alternatively use inter-vertebral disc labels with the analogous procedure of reference numbered voxels.

We perform this step on 3D T1w images in order to achieve better accuracy given their higher overall quality and contrast compared to DKI ones, where vertebral discs are not clearly identifiable.

Labeling from 3D T1w anatomical image is possible as it turned out to match relatively well along the superior-inferior (z) axis, the target direction of disc labeling, with the DKI scan (not along the Anterior-Posterior (AP) or Right-Left (RL) direction, Figure 4).

Vertebral labeling is typically done using an automatic method *sct_label_vertebrae*, that finds C2-C3 disc, and then locates neighbouring discs using similarity measure with the PAM50 template at each specific level (Ullmann et al., 2014).

Default SCT procedure *sct_label_vertebrae* fails in automatically detecting C2-C3 vertebral disc once again because of the small size of spines at issue and low image contrast compared to adults.

Therefore, we manually create labels with the command *sct_label_utils* through interactive viewer option provided by SCT (flag -*create-viewer*) with little to no waste of time.

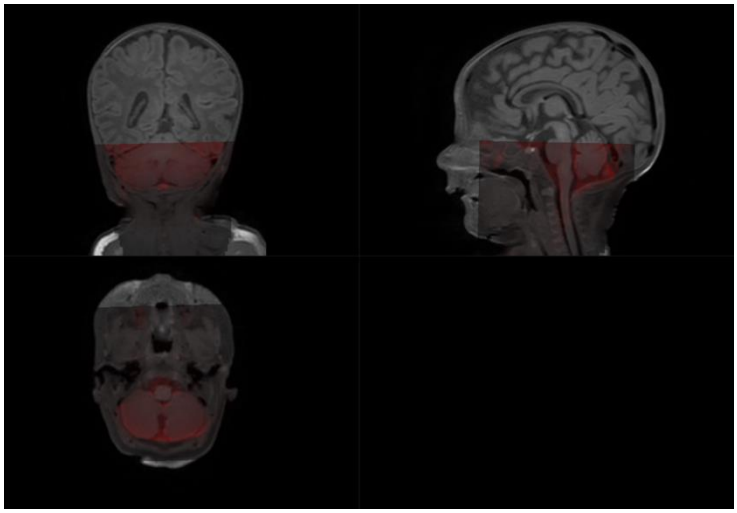

Figure 4. DKI scan overlaid on structural 3dT1w image: while both images are clearly not registered along the antero-posterior direction due to the very strong susceptibility artefact, the z-location is similar: see how the bottom tip of the cerebellum is consistent for the two scans

2.4.2. Registration to PAM50 atlas

Registration between subject's diffusion and atlas space is a very demanding task in case of neonatal imaging given the lack of a specific pediatric atlas compatible with SCT (one is currently under creation, https://github.com/neuropoly/spinalcordtoolbox/issues/2530). We thus use PAM50 atlas (de Leener et al., 2018), an adult template for MRI of the full SC and brainstem in the same coordinate system as the ICBM152 (MNI) brain template, allowing to conduct simultaneous brain/spine studies. It consists of a T1w, T2w, T2*w, white and gray matter probabilistic atlas and white matter atlas of

tracts as well as probabilistic labeling of spinal levels. The template has been constructed from straightened SC for facilitating registration and visualization of results.

sct_register_to_template is the main command for registering one subject to the template and vice versa, since it outputs the forward and backward warping fields. We choose subject's native diffusion space as target of registration transforms since the straightening required by opposite strategy would cause through-plane interpolation errors which would bias following extraction of diffusion measures (de Leener et al., 2017b).

Moreover, we suggest employing T1w atlas image for its better contrast similarity with DKI scan compared to T2w.

Application of default command does not produce satisfactory results, stressing the need to tweak all input parameters to deal with our particular contrast and resolution. Given the presence of artifacts and some inherent features (e.g., low CSF/cord contrast) that could compromise the registration, we use SC segmentation as input for the algorithm in order to ensure maximum robustness.

Registration is then built through multiple steps by increasing the complexity of the transformation performed in each step (starting with large deformation with low degree of freedom and finishing with local adjustment). The first step consists in vertebral alignment, that is vertebral level matching between the subject and the template on the basis of posterior edge of the intervertebral discs provided by previous manual vertebral labeling. Second step is slice-wise center of mass alignment between the two images, using *centermass* algorithm instead of default *centermassrot* (which also includes rotation alignment) because the cord is quasi-circular and cord angle estimation is not reliable here. The third step is R-L scaling along x axis followed by A-P alignment to match segmentation borders along y axis, with the ultimate aim of accommodating the very small SC size. Finally, iterative slice-wise non-linear registration is performed through non-linear symmetric normalization regularized with b-splines (Tustison and Avants, 2013) using information from comparison of Cross Correlation metric (CC) between the two images, which allows SC shape refinement. Once the algorithm completed, one can assess the quality of registration through visual evaluation and inspection of QC module, and thus warp the template and all its objects to each subject's DKI image (Figure 5).

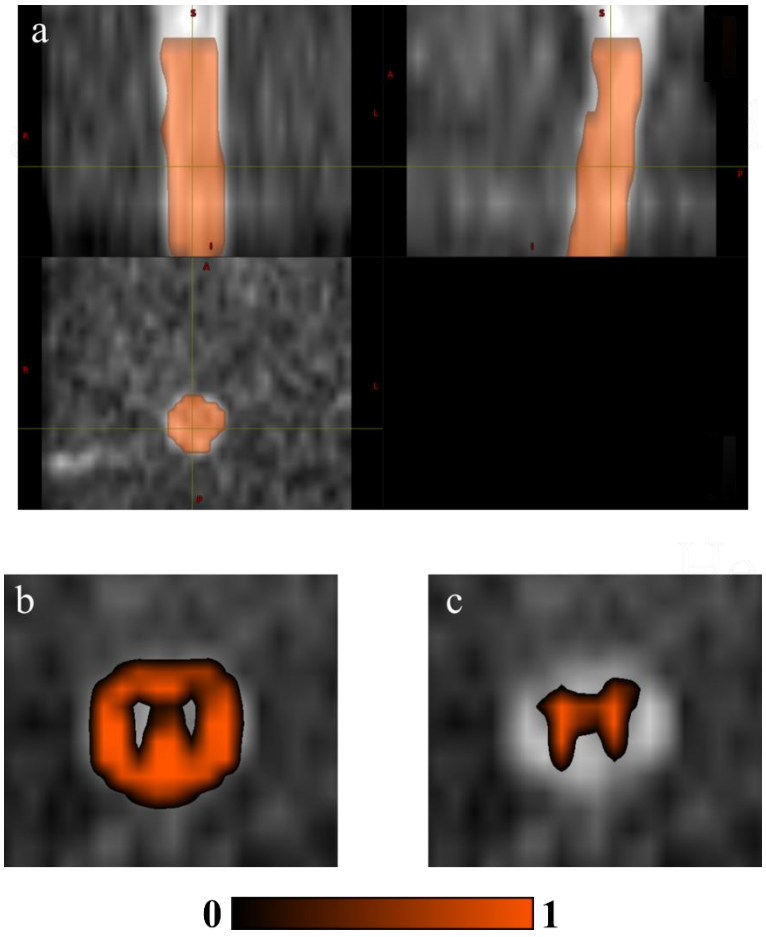

Figure 5. Registration with PAM50 atlas and ROI detection through atlas-based approach: (a) PAM50 atlas' cord segmentation binary mask, (b) WM and (c) GM probabilistic masks warped to subject's DKI motion-corrected image

2.4.3. Computation of diffusion metrics

The end point of previous preprocessing and processing steps is computation of diffusion parametric maps, from which to extract quantitative summary measures requested by the particular study in question. We estimate diffusion parametric maps through DIPY software (v. 1.1.1). To avoid unnecessary calculations on the background of the image, we use a mask created by dilating spinal cord segmentation (through *sct_maths* command) because values outside the binary cord mask are important for proper account of PVE, having to be minimized in every possible way (Lévy et al., 2015). Indeed, this phenomenon, because of the coarse resolution of MRI with respect to SC anatomy, may make the apparent value within a boundary voxel be a mixture between the WM and CSF compartment, thus yielding a subsequent inaccurate quantification of diffusion measures.

Since DKI model involves the estimation of a large number of parameters (Tax et al., 2015) and is more sensitive to artefacts (Neto Henriques, 2012) , we choose to suppress the effects of noise and artefacts before diffusion kurtosis fitting using a 3D Gaussian smoothing (with a Gaussian kernel with fwhm=1.25) as suggested by pioneer DKI studies (Jensen et al., 2005).

DTI measures are computed from kurtosis tensor model as they are expected to have better accuracy (Veraart et al., 2011). The following parametric maps can thus be generated: Mean Diffusivity (MD), Axial Diffusivity (AD), Radial Diffusivity (RD), Fractional Anisotropy (FA) and Mean Kurtosis (MK), Axial Kurtosis (AK), Radial Kurtosis (RK), Kurtosis Fractional Anisotropy (KFA), displayed in Figure 1S.

MD measures the average diffusivity within a voxel and thus represents the overall magnitude of diffusion; AD indicates the amount of diffusivity along the principal diffusion direction and relates to axonal architecture; RD, probing diffusion along the direction perpendicular to the main one, is a marker of myelin integrity; finally, FA quantifies the degree of diffusion anisotropy within the voxel and stands for microstructural organization and WM integrity (Alexander et al., 2007). As regards biophysical interpretation of corresponding DKI measures, MK reflects the overall microstructural complexity and voxel compartmentalization; AK measures the kurtosis in the direction of the principal diffusion tensor eigenvector and stands for microstructural complexity along the axons; RK could be representative of the degree of axonal and myelin integrity (Steven et al., 2014); KFA assesses the directional variation in the degree of non-Gaussian diffusion (Hansen, 2019).

Postprocessing

Thanks to this atlas-based analysis approach, it is possible to perform cord-specific quantification of diffusion metrics through *sct_extract_metric* command, also restricted to specific Regions of Interest (ROIs; labels used by default are taken from the PAM50 template, e.g. WM tracts, flag -*l*), vertebral levels (flag -*vert*) or slice (flag -*z*), according to the specific clinical needs concerned.

Along with WM and GM probabilistic masks as a whole (Figure 5 b,c), normally investigated in medical practice, one can carry out ROI detection also in specific tracts according to the clinical question (fifteen WM tracts and three GM regions available in total for each side).

Data and code availability

Data used in this study is not able to be made openly available due to privacy restrictions of clinical data imposed by the Gaslini Hospital's administration. Regarding code availability, a specific pipeline compatible with SCT is integrated in an open-access GitHub repository within "SCT-pipeline", a site gathering various pipelines compatible with SCT for processing MRI data (https://github.com/sct-pipeline/pediatric-genova).

3. Case Study

3.1. Clinical question

In order to test the overall quality of the pipeline, we analyzed both DTI and DKI metrics of cSC in a cohort of preterm infants studied at term-equivalent age.

Periventricular WM Injury (PMWI) is the most frequent type of brain lesion in preterm infants, and the spatial extent and location of WM injury correlate with distinct clinical outcomes, including cerebral palsy and motor impairment (Volpe et al., 2017).

Given the strong association of WM injury with the motor function development of preterm neonates, we assessed the hypothesis that the presence of periventricular punctate WM lesions identified on MRI at term-equivalent age could be associated with regionally specific alterations in cSC microstructure.

A similar approach was already used by (Panara et al., 2019) to characterize cSC microstructural abnormalities in a cohort of adult patients with previous unilateral ischemic stroke in the vascular territory of the middle cerebral artery (MCA). DTI and DKI diffusion measures in cSC resulted to be a valuable imaging marker for predicting clinical outcome. In particular, significant reduction of FA and MK was observed in the affected lateral WM bundle of the cSC, correlating with the severity of motor dysfunction.

Accordingly, the ultimate goal of our study was to verify whether the presence of periventricular WM lesions affects the cSC tracts development. Specifically, we aimed to compare DTI and DKI measures of cSC in two groups of preterm neonates: i) with punctate Periventricular White Matter lesions (PWMI), and ii) with normal brain MRI (controls).

3.2. Materials and Methods

Subjects have been enrolled since August 2019 and scanned with 3.0 T MR scanner using a 32-channel head array coil (Ingenia Cx, Philips, Best, the Netherlands) at the Neuroradiology Unit of Gaslini Children's Hospital making use of aforementioned acquisition protocol. Conventional MRI and DKI were performed in 13 pre-term infants (28 to 35 weeks Gestational Age [GA]; scanned at term-equivalent age).

This single-center study was carried out in accordance with the recommendations of "Comitato Etico Regione Liguria, Genoa, Italy" with written informed parental consent obtained for each infant prior to examination in accordance with the Declaration of Helsinki. Patients were fed before MRI examination to achieve spontaneous sleep and were spontaneously breathing during examination. Heart rate and oxygen saturation were non-invasively monitored. Oxygen saturation ranged between 97 and 99% in all neonates during the examinations.

Exclusion criteria included obvious motion artifacts, oblique positioning, an incomplete imaging process or a low SNR. We opted for focusing exclusively on upper SC portion, by only acquiring the cervical district (C1-C7), affected by a significantly lower degree of physiologic motion than the dorsal and lumbar portions (Yang et al., 2010).

In consensus with a board-certified pediatric neuroradiologist, we performed QC for each of the pipeline's steps.

FOV reduction allowed to exclude upper non-spinal areas (i.e. cerebellum) as well as lower spinal levels whose corresponding slices are not usable due to poor image quality.

To validate the quality of segmentation, we checked the QC feature and noticed some local segmentation leakage in a few slices for two subjects and hence corrected it manually.

Vertebral labeling was created at the posterior tip of the top of C1 vertebra and at C3-C4 disc, centered in the cord. Manual intervention only took a few seconds per subject (Figure 3S).

Atlas registration algorithm robustly achieved convergence as verified through inspection of QC feature.

Neither DKI nor structural images ensured sufficient WM-GM-CSF contrast to perform any manual detection of ROIs in contrast to high-contrast PSIR image of (Panara et al., 2019), whose acquisition time would be too long for neonates. Therefore, we exploited good registration outcome for automatic delineation of ROIs through atlas-based approach.

We opted for using lateral CSTs as ROIs for consistency with (Panara et al., 2019) - though grouping together left and right sides in order to gain robustness by increasing volume fraction as suggested in (de Leener et al., 2017a) - as well as WM and GM.

We then computed averages of diffusion measures across C1-C4 vertebral levels in order to avoid a subject-based bias: outside of these levels the registration is inaccurate and/or MRI signal may be corrupted. We thus checked through QC module the correctly segmented slices corresponded to the same vertebral levels across subjects, starting from the first slice containing only SC (excluding cerebellum, Figure 2Sc).

Moreover, estimation of DTI and DKI weighted average metrics was limited to those slices where spinal cord segmentation is accurate: outside segmentation mask, metrics would indeed be irrelevant. This was obtained by multiplying segmentation mask by specific WM, GM and CSTs atlas labels. We quantified diffusion metrics using Weighted Average (WA) estimation to minimize PVE avoiding bias into resulting metrics by the surrounding tissues (e.g. CSF). This is one of the recommended methods especially in case of noisy images and small tracts as in our case. We assessed associated voxel fraction to quantify the reliability of our diffusion measures: as demonstrated in (de Leener et al., 2017a), having at least 240 voxels results in an error smaller than 1%, while having 30 voxels results in an error inferior than 2%. In this example, the metrics were computed based on average 173, 50 and 32 voxels in WM, GM and CSTs respectively, thus assuring sufficient accuracy of estimates.

3.3. Results

3.3.1. Population size and classification

In order to investigate clinical differences among acquired subjects, we grouped infants as follows: i) 8 subjects with punctate PWMI and ii) 4 subjects with normal brain MRI, used as control group.

At QC phase, in accordance with the expert neuroradiologist, we opted for excluding one control subject due to excessively poor image quality (i.e. signal leakage at C1-C3 level, Figure 2Sa,b).

Therefore, the final number of subjects under analysis amounted to 8 and 3 infants for the two groups, respectively.

3.3.2. Trend of diffusion measures

For consistency with (Panara et al., 2019), Figure 6 reports trend of cSC FA and MK measures in the two groups of neonates.

For the sake of completeness, in Figure 4S we include all metrics, the most familiar DTI ones and the most recent DKI measures.

To an initial evaluation based on the limited sample size available, considering the variation of average metrics between controls and patients in WM, we can notice a decrease in MD, AD, FA, MK, and KFA, parallel to an overall increase in RD and AK in preterm neonates with PWMI.

As regards GM, MK, AK and RK exhibit an upward trend, as opposed to MD, AD, FA and KFA.

Secondly, we observe an overall reduction in standard deviation in the largest group of neonates (PWMI), which suggests high reproducibility for the majority of computed diffusion metrics.

Finally, range of values of DTI measures are consistent with normative values on healthy pediatric SC (Singhi et al., 2012). MD, AD and RD values are higher while FA values are lower compared to equivalent measures on older cohorts of patients (i.e. children/ adolescents, (Alizadeh et al., 2018b; Mulcahey et al., 2013; Saksena et al., 2018a, 2016)). This trend is in line with the simultaneous age-related decrease in MD, AD and RD and increase in FA metrics reflecting progressive maturation, myelination and fiber packing and thickening within the SC, similar to that observed in the brain (Pierpaoli et al., 1996; Pierpaoli and Basser, 1996).

Conversely, definition of a normative variation of DKI measures across age from newborns to adults will be feasible after further investigations from early stages of development.

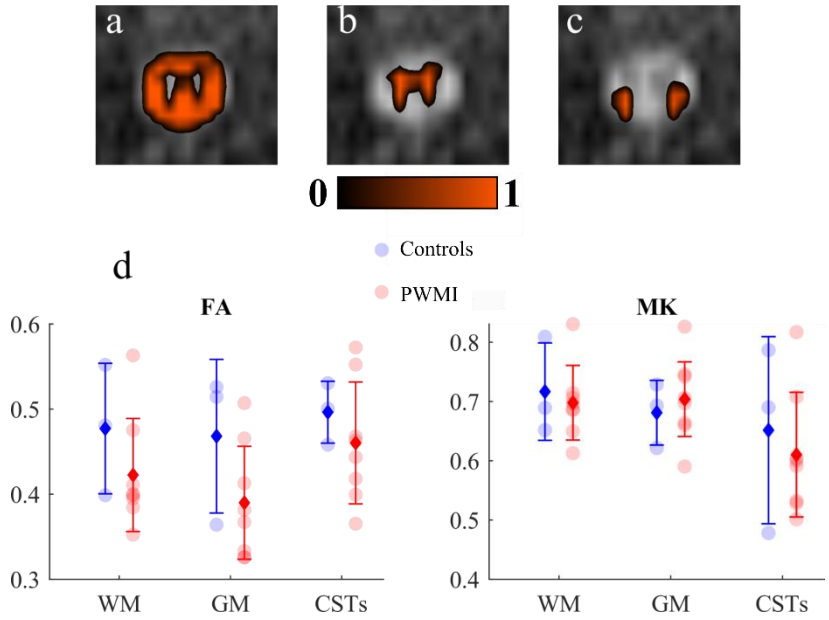

Figure 6. Extraction of diffusion measures within ROIs: (a) White Matter (WM), (b) Gray Matter (GM) and (c) Cortico-Spinal Tracts (CSTs) ROIs overlaid on DKI motion corrected image; (d) Scatter plots of FA and MK in group subjects across aforementioned ROIs: colored spots indicate single subject's value for each metric; as reported in the legend, controls' measures are in blue, whereas Periventricular White Matter Injury (PWMI) group's in red. Units for MK are in mm^2/s while FA is dimensionless. Error bars displaying mean (diamond) and standard deviation are overlaid on scatter plots.

4. Discussion

4.1. Research question

The motivation behind the present work draws on the lack of studies concerning analysis of neonatal SC data through advanced dMRI techniques like DKI. Indeed, it is worth facing challenges resulting from conflicting imaging requirements of neonatal age range and state-of-the-art diffusion strategies, respectively. Possibility of successfully exploiting increased sensitivity and sensibility inherent to DKI methodology also into neonatal setting would indeed be extremely useful for throwing light on complex diseases related to this critical phase of development and to deepen the knowledge about the relationship between brain and SC at birth.

4.2. Study significance

Here we present the first application of DKI to neonatal SC through a pipeline able to perform complete processing on a subject within a clinically acceptable time (10 minutes average with the current setup). As regards acquisition setting, we were able to perform a time-consuming technique like DKI using a short diffusion sequence which minimizes patient's physiological motion and which likely reflects a standard clinical scenario devoid of latest technologies in terms of acquisition sequence optimization. With regard to image processing, we opted for creating this pipeline using SCT since it represents the only existing comprehensive, free and open-source software dedicated to the processing and analysis of SC multi-parametric MRI data. Adaptation of each image processing tools already in use for adult subjects through appropriate tuning of parameters turned out to be feasible and allowed to successfully overcome all the issues mentioned in the 'Introduction' section inherent to imaging of SC and exacerbated in case of neonatal setting, even for the most challenging steps like segmentation or registration to atlas. We were thus able to quantify diffusion measures within specific ROIs using an atlas-based approach which presents undisputed advantages compared to usual manual drawing of ROIs: it is automatic and thus highly reproducible, it is not biased by the user experience and knowledge of the anatomy, it is much faster than long and tedious manual delineation of ROIs and it allows to account for PVE unlike manual ROIs consisting in binary masks. Preliminary application of our method to a limited number of subjects has yielded physiologically plausible findings. In particular, differences in DTI and DKI measures observed between PWMI neonates and controls confirm the hypothesis that PWM injuries in the premature brain can be associated with microstructural alterations of both GM and WM of neonatal cSC at term-equivalent age. These findings also highlight the importance of complementary analysis of DTI and DKI metrics for a more accurate characterization of biological tissues. Further analyses on a wider cohort of neonates are necessary to confirm these preliminary results, and specifically to prove if microstructural changes in cSC in preterm neonates with PWMI correlate with clinical and neurological outcome.

4.3. Added value of DKI

Results about feasibility of DTI and DKI analysis in neonatal SC with subjects collected so far are preliminary but promising.

It is interesting to note how a DKI metric such as KFA, although yet underused in clinical studies, proves to be sensitive to microstructural changes in PWMI subjects by reducing its value in all considered ROIs. Indeed, this measure has been recently discovered to reflect tissue-diffusion complexity managing to provide contrast in areas where FA does not (Hansen, 2019).

Another crucial point of reflection concerns observing how the presence of a WM lesion in the brain causes subsequent alterations not only in cSC WM but also GM, as evidence of the strong association between brain and spine. In this respect, resorting to DKI measures becomes of utmost importance given kurtosis sensitivity to structural changes in isotropic tissues such as GM. Indeed, while it is easy to notice WM values are higher than corresponding GM values for the majority of DTI measures both in healthy and unhealthy group, this trend shows grater variability in case of DKI, whose most of the metrics show comparable WM-GM values.

Moreover, range of variation of DKI metrics from controls to PWMI is overall higher in GM than that of corresponding DTI measures.

This is an expected finding: DTI is extremely suitable for capturing highly directional diffusion typical of WM bundles but shows low sensitivity to isotropic diffusion, whereas DKI allows specific assessment of non-gaussian diffusion typical of GM areas (Paydar et al., 2014).

Such findings once again stress the importance of combining DTI and DKI metrics as complementary sensitive biomarkers in order to fully exploit the potential of dMRI compared to conventional MRI.

However, a more comprehensive corroboration and explanation of our results is expected after collecting an adequate number of subjects to carry out a robust statistical survey. An in-depth interpretation of the single metrics is out of the scope of this paper. Here, we just dwell on exploring the comparison with the work on adults which served as a starting point.

4.4. Comparison with corresponding adult study

Both FA and MK trend agree with (Panara et al., 2019). FA exhibits a reduction in WM, GM and CSTs in case of pathology, whereas MK only decreases in WM and CSTs tracts (Figure 6).

Since FA is known to be an index of structural integrity (Hansen, 2019) and MK a marker of tissue microstructure complexity (Jensen et al., 2005), obtained findings suggest that, in case of overlying WM brain lesion, a loss of integrity and complexity is registered also in SC WM tracts below with a

more isotropic diffusion pattern due to disruption of white matter tracts. This biologically plausible hypothesis already verified for adults would also subsist in infants.

4.5. Study limitations

Present pipeline has been designed with current instruments at disposal and with given data whose resolution is high in axial plane but whose contrast is very low due to short acquisition time: with any improvement in acquisition setup our pipeline will bring to even stronger and more comprehensive results.

Major flaws of this procedure consist in basing on an adult atlas, where the exact location of tracts may not perfectly correspond to neonatal images despite the good adjustment of registration parameters. Current pipeline will definitely benefit from introduction of a pediatric atlas into SCT. Moreover, image quality could be further improved: scans we acquired are all the same prone to noise and artifacts due to short acquisition time dictated by clinical needs and to the lack of specific spatially-selective MR sequences. Starting from more advanced hardware tools may significantly increase image quality and thus accuracy of estimated metrics.

4.6. Future developments

Validation of current pipeline can be made by testing it to a larger cohort of subjects, possibly investigating also lower SC tracts, including thoracic and lumbar districts, and extending studies to different clinical cases, preferably focusing on a determined pathology. For example, it would be interesting to explore correlations between DKI measures and specific clinical scores as done in (Panara et al., 2019) where diffusion measures have been related to motor performance indexes.

A further step may be adapting this analysis pipeline to other promising higher-order diffusion models requiring multi-shell acquisition such as NODDI (Zhang et al., 2012).

5. Conclusion

Proper acquisition protocol combined with accurate adjustment of processing algorithms customized for adult SC opens up new horizons in exploiting increased ability of advanced dMRI models, such

as DKI, in providing a closer insight into both GM and WM microstructure of SC also in neonatal domain, where they had never been utilized before.
This semi-automated pipeline hence paves the wave for applying advanced dMRI models to neonatal setting in a wide range of potential clinical applications.

Declaration of interest

Declarations of interest: none

Author contributions

Rosella Trò: Conceptualization, Methodology, Software, Writing - Original Draft, Visualization. **Monica Roascio**: Conceptualization, Supervision. **Domenico Tortora**: Conceptualization, Validation, Investigation, Resources, Supervision. **Mariasavina Severino**: Validation, Investigation, Resources, Supervision. **Andrea Rossi:** Validation, Investigation, Resources, Supervision. **Julien Cohen-Adad:** Writing- Reviewing and Editing, Supervision. **Marco Massimo Fato:** Conceptualization, Writing- Reviewing and Editing, Supervision. **Gabriele Arnulfo:** Conceptualization, Writing- Reviewing and Editing, Supervision. **These last two authors contributed equally.**

Funding sources

This research did not receive any specific grant from funding agencies in the public, commercial, or not-for-profit sectors.

Acknowledgements

The authors would like to thank Prof. Luca Antonio Ramenghi (Neonatal Intensive Care Unit, IRCCS Istituto Giannina Gaslini, Genoa, Italy e Department of Neurosciences, Rehabilitation, Ophthalmology, Genetics, Maternal and Child Health (DINOGMI), University of Genoa, Italy) and the LIFT (Laboratorio di Imaging Funzionale 3 Tesla).

Supplementary material

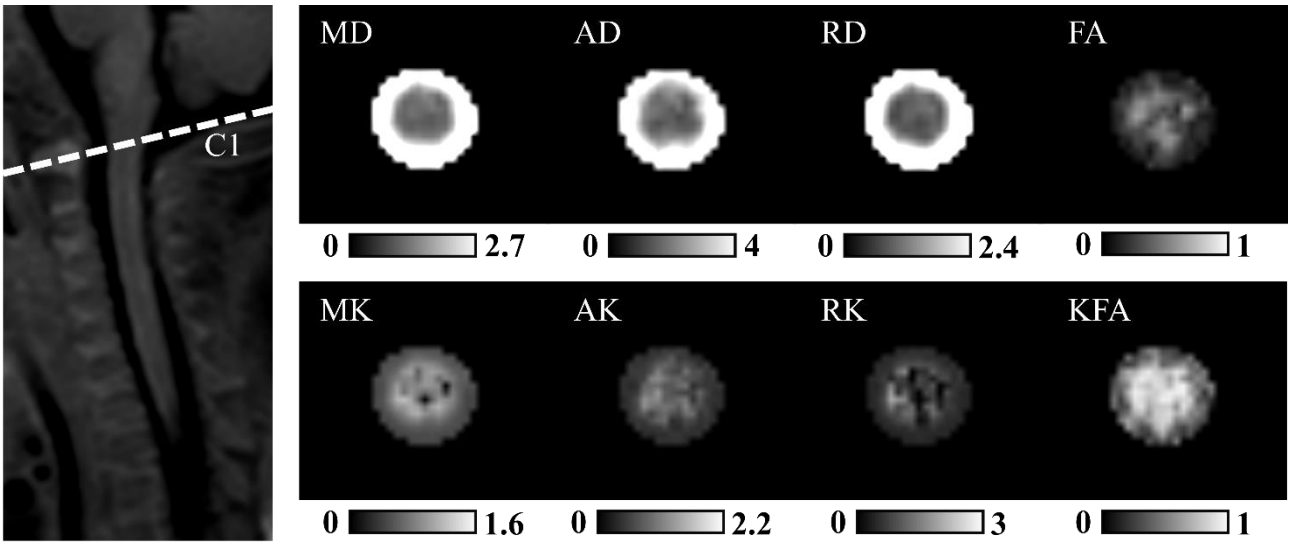

Figure 1S. Diffusion and kurtosis maps at the mid-C1 level for one example subject: Units for MD, AD and RD are $\mu m^2/s$; for MK, AK and RK mm^2/s; while FA and KFA are dimensionless.

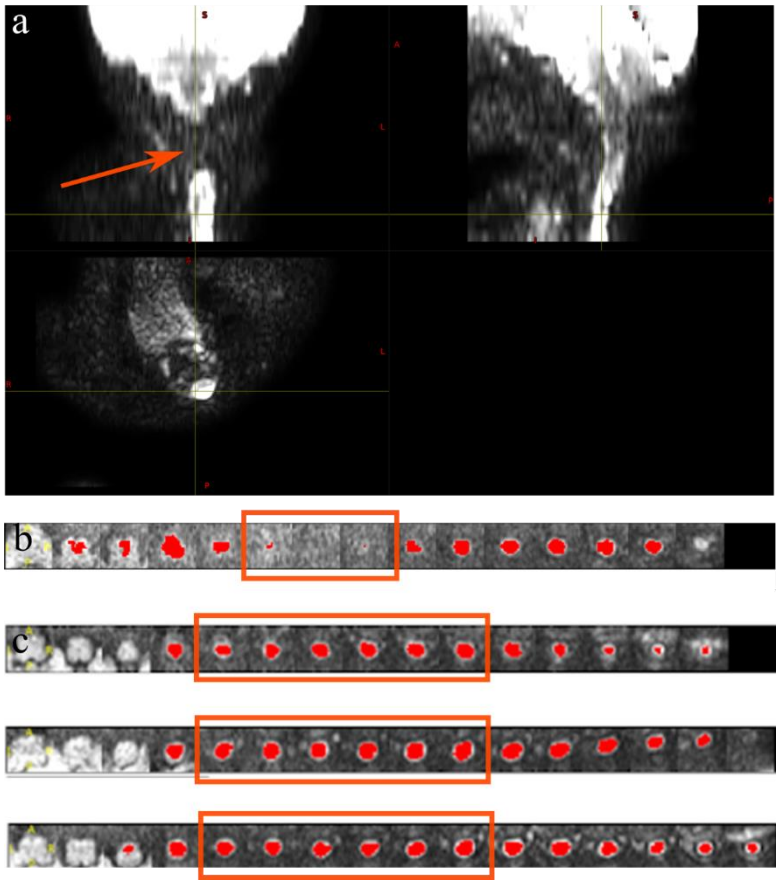

Figure 2S. Quality control: (a) Example of excluded DKI scan and (b) relative SC segmentation show signal loss across multiple slices as the coronal plane is not overlapping with the cord (ie: lordosis); (c) QC of C1-C3 levels: axial slices under analysis correspond to the same cervical levels for all subjects as shown in three example subjects.

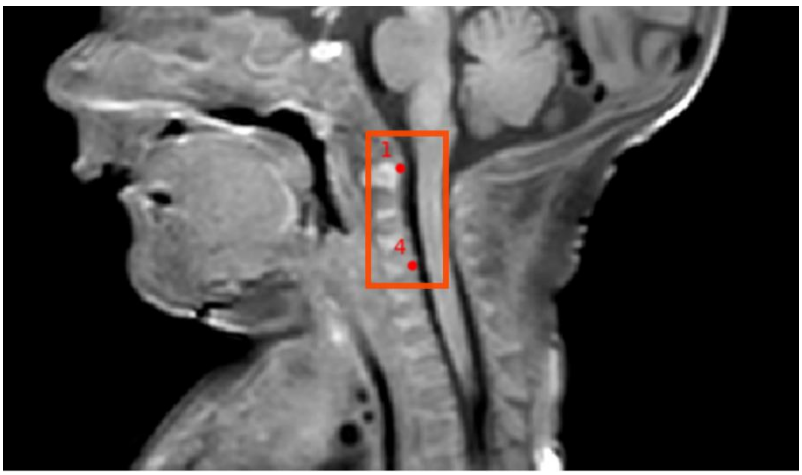

Figure 3S. Vertebral labeling: Manual labeling of top of C1 vertebra and C3-C4 disc from graphical user interface integrated in SCT

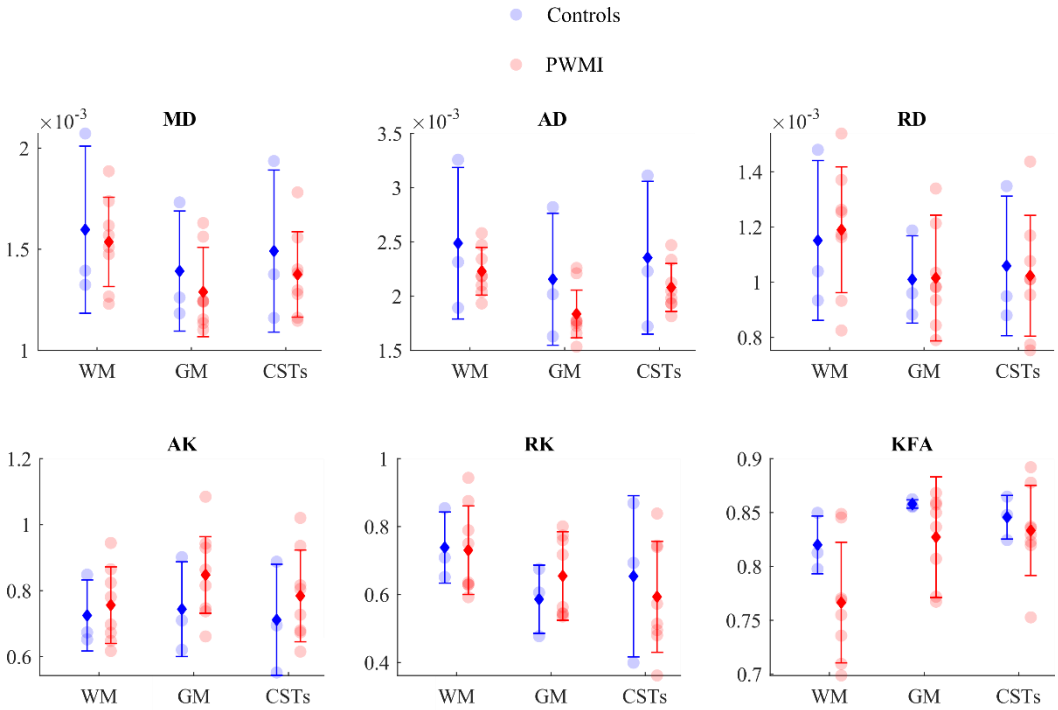

Figure 4S. Extraction of diffusion measures within ROIs: Scatter plots of DTI and DKI measures in group subjects across aforementioned ROIs: coloured spots indicate single subject's value for each metric; as reported in the legend, controls' measures are in blue, whereas Periventricular White Matter Injury (PWMI) group's in red. Units for MD, AD, RD, MK, AK and RK are in mm^2/s, while FA and KFA are dimensionless. Error bars displaying mean (diamond) and standard deviation are overlaid on scatter plots.

References

Alexander, A.L., Lee, J.E., Lazar, M., Field, A.S., 2007. Diffusion Tensor Imaging of the Brain. Neurotherapeutics. https://doi.org/10.1016/j.nurt.2007.05.011

Alizadeh, M., Fisher, J., Saksena, S., Sultan, Y., Conklin, C.J., Middleton, D.M., Finsterbusch, J., Krisa, L., Flanders, A.E., Faro, S.H., Mulcahey, M.J., Mohamed, F.B., 2018a. Reduced Field of View Diffusion Tensor Imaging and Fiber Tractography of the Pediatric Cervical and Thoracic Spinal Cord Injury. Journal of Neurotrauma. https://doi.org/10.1089/neu.2017.5174

Alizadeh, M., Fisher, J., Saksena, S., Sultan, Y., Conklin, C.J., Middleton, D.M., Krisa, L., Finsterbusch, J., Flanders, A.E., Faro, S.H., Mulcahey, M.J., Mohamed, F.B., 2018b. Age related diffusion and tractography changes in typically developing pediatric cervical and thoracic spinal cord. NeuroImage: Clinical. https://doi.org/10.1016/j.nicl.2018.03.014

Andre, J.B., Bammer, R., 2010. Advanced diffusion-weighted magnetic resonance imaging techniques of the human spinal cord. Topics in Magnetic Resonance Imaging. https://doi.org/10.1097/RMR.0b013e31823e65a1

Antherieu, P., Levy, R., de Saint Denis, T., Lohkamp, L., Paternoster, G., di Rocco, F., Boddaert, N., Zerah, M., 2019. Diffusion tensor imaging (DTI) and Tractography of the spinal cord in pediatric population with spinal lipomas: preliminary study. Child's Nervous System. https://doi.org/10.1007/s00381-018-3935-2

Barth, M., Breuer, F., Koopmans, P.J., Norris, D.G., Poser, B.A., 2016. Imaging Methodology - Review Simultaneous Multislice (SMS) Imaging Techniques. Magnetic Resonance in Medicine.

Battiston, M., Grussu, F., Ianus, A., Schneider, T., Prados, F., Fairney, J., Ourselin, S., Alexander, D.C., Cercignani, M., Gandini Wheeler-Kingshott, C.A.M., Samson, R.S., 2018. An optimized framework for quantitative magnetization transfer imaging of the cervical spinal cord in vivo. Magnetic Resonance in Medicine. https://doi.org/10.1002/mrm.26909

Bester, M., Sigmund, E., Tabesh, A., Jaggi, H., Inglese, M., Mitnick, R., 2010. Diffusional Kurtosis Imaging of the cervical spinal cord in multiple sclerosis patients. Proc. Intl. Soc. Mag. Reson. Med.

Bester, M., Sigmund, E., Tabesh, A., Jaggi, H., Inglese, M., Mitnick, R., 2009. Diffusional Kurtosis Imaging of the cervical spinal cord in multiple sclerosis patients.

Brooks, J.C.W., Büchel, C., Winkler, A.M., Andersson, J.L., Tracey, I., 2017. Investigating resting-state functional connectivity in the cervical spinal cord at 3 T. NeuroImage. https://doi.org/10.1016/j.neuroimage.2016.12.072

Castellano, A., Papinutto, N., Cadioli, M., Brugnara, G., Iadanza, A., Scigliuolo, G., Pareyson, D., Uziel, G., Köhler, W., Aubourg, P., Falini, A., Henry, R.G., Politi, L.S., Salsano, E., 2016. Quantitative MRI of the spinal cord and brain in adrenomyeloneuropathy: In vivo assessment of structural changes. Brain. https://doi.org/10.1093/brain/aww068

Conklin, C.J., Middleton, D.M., Alizadeh, M., Finsterbusch, J., Raunig, D.L., Faro, S.H., Shah, P., Krisa, L., Sinko, R., Delalic, J.Z., Mulcahey, M.J., Mohamed, F.B., 2016. Spatially selective 2D RF inner field of view (iFOV) diffusion kurtosis imaging (DKI) of the pediatric spinal cord. NeuroImage: Clinical. https://doi.org/10.1016/j.nicl.2016.01.009

de Leener, B., Fonov, V.S., Collins, D.L., Callot, V., Stikov, N., Cohen-Adad, J., 2018. PAM50: Unbiased multimodal template of the brainstem and spinal cord aligned with the ICBM152 space. NeuroImage. https://doi.org/10.1016/j.neuroimage.2017.10.041

de Leener, B., Kadoury, S., Cohen-Adad, J., 2014. Robust, accurate and fast automatic segmentation of the spinal cord. NeuroImage. https://doi.org/10.1016/j.neuroimage.2014.04.051

de Leener, B., Lévy, S., Dupont, S.M., Fonov, V.S., Stikov, N., Louis Collins, D., Callot, V., Cohen-Adad, J., 2017a. SCT: Spinal Cord Toolbox, an open-source software for processing spinal cord MRI data. NeuroImage. https://doi.org/10.1016/j.neuroimage.2016.10.009

de Leener, B., Mangeat, G., Dupont, S., Martin, A.R., Callot, V., Stikov, N., Fehlings, M.G., Cohen-Adad, J., 2017b. Topologically preserving straightening of spinal cord MRI. Journal of Magnetic Resonance Imaging. https://doi.org/10.1002/jmri.25622

Duval, T., Lévy, S., Stikov, N., Cohen-Adad, J., Stikov, N., Campbell, J., Mezer, A., Witzel, T., Keil, B., Smith, V., Wald, L.L., Klawiter, E., Lévy, S., Cohen-Adad, J., 2017. g-Ratio weighted imaging of the human spinal cord in vivo. NeuroImage. https://doi.org/10.1016/j.neuroimage.2016.09.018

Eippert, F., Kong, Y., Jenkinson, M., Tracey, I., Brooks, J.C.W., 2017. Denoising spinal cord fMRI data: Approaches to acquisition and analysis. NeuroImage. https://doi.org/10.1016/j.neuroimage.2016.09.065

Farquharson, S., Tournier, J.D., Calamante, F., Fabinyi, G., Schneider-Kolsky, M., Jackson, G.D., Connelly, A., 2013. White matter fiber tractography: Why we need to move beyond DTI. Journal of Neurosurgery. https://doi.org/10.3171/2013.2.JNS121294

Fruehwald-Pallamar, J., Szomolanyi, P., Fakhrai, N., Lunzer, A., Weber, M., Thurnher, M.M., Pallamar, M., Trattnig, S., Prayer, D., Noebauer-Huhmann, I.M., 2012. Parallel imaging of the cervical spine at 3T: Optimized trade-off between speed and image quality. American Journal of Neuroradiology. https://doi.org/10.3174/ajnr.A3101

Garyfallidis, E., Brett, M., Amirbekian, B., Rokem, A., van der Walt, S., Descoteaux, M., Nimmo-Smith, I., 2014. Dipy, a library for the analysis of diffusion MRI data. Frontiers in Neuroinformatics. https://doi.org/10.3389/fninf.2014.00008

Grabher, P., Mohammadi, S., Trachsler, A., Friedl, S., David, G., Sutter, R., Weiskopf, N., Thompson, A.J., Curt, A., Freund, P., 2016. Voxel-based analysis of grey and white matter degeneration in cervical spondylotic myelopathy. Scientific Reports. https://doi.org/10.1038/srep24636

Gros, C., de Leener, B., Badji, A., Maranzano, J., Eden, D., Dupont, S.M., Talbott, J., Zhuoquiong, R., Liu, Y., Granberg, T., Ouellette, R., Tachibana, Y., Hori, M., Kamiya, K., Chougar, L., Stawiarz, L., Hillert, J., Bannier, E., Kerbrat, A., Edan, G., Labauge, P., Callot, V., Pelletier, J., Audoin, B., Rasoanandrianina, H., Brisset, J.C., Valsasina, P., Rocca, M.A., Filippi, M., Bakshi, R., Tauhid, S., Prados, F., Yiannakas, M., Kearney, H., Ciccarelli, O., Smith, S., Treaba, C.A., Mainero, C., Lefeuvre, J., Reich, D.S., Nair, G., Auclair, V., McLaren, D.G., Martin, A.R., Fehlings, M.G., Vahdat, S., Khatibi, A., Doyon, J., Shepherd, T., Charlson, E., Narayanan, S., Cohen-Adad, J., 2019. Automatic segmentation of the spinal cord and intramedullary multiple sclerosis lesions with convolutional neural networks. NeuroImage. https://doi.org/10.1016/j.neuroimage.2018.09.081

Hansen, B., 2019. An Introduction to Kurtosis Fractional Anisotropy. AJNR. American journal of neuroradiology 40, 1638–1641. https://doi.org/10.3174/ajnr.A6235

Hori, M., Hagiwara, A., Fukunaga, I., Ueda, R., Kamiya, K., Suzuki, Y., Liu, W., Murata, K., Takamura, T., Hamasaki, N., Irie, R., Kamagata, K., Kumamaru, K.K., Suzuki, M., Aoki, S., 2018. Application of Quantitative Microstructural MR Imaging with Atlas-based Analysis for the Spinal Cord in Cervical Spondylotic Myelopathy. Scientific Reports. https://doi.org/10.1038/s41598-018-23527-8

Huber, E., David, G., Thompson, A.J., Weiskopf, N., Mohammadi, S., Freund, P., 2018. Dorsal and ventral horn atrophy is associated with clinical outcome after spinal cord injury. Neurology. https://doi.org/10.1212/WNL.0000000000005361

Jensen, J.H., Helpern, J.A., Ramani, A., Lu, H., Kaczynski, K., 2005. Diffusional kurtosis imaging: The quantification of non-Gaussian water diffusion by means of magnetic resonance imaging. Magnetic Resonance in Medicine. https://doi.org/10.1002/mrm.20508

Kaplan, K.M., Spivak, J.M., Bendo, J.A., 2005. Embryology of the spine and associated congenital abnormalities. Spine Journal. https://doi.org/10.1016/j.spinee.2004.10.044

Kong, Y., Eippert, F., Beckmann, C.F., Andersson, J., Finsterbusch, J., Büchel, C., Tracey, I., Brooks, J.C.W., 2014. Intrinsically organized resting state networks in the human spinal cord. Proceedings of the National Academy of Sciences of the United States of America. https://doi.org/10.1073/pnas.1414293111

Lévy, S., Benhamou, M., Naaman, C., Rainville, P., Callot, V., Cohen-Adad, J., 2015. White matter atlas of the human spinal cord with estimation of partial volume effect. NeuroImage. https://doi.org/10.1016/j.neuroimage.2015.06.040

Li, D., Wang, X., 2017. Application value of diffusional kurtosis imaging (DKI) in evaluating microstructural changes in the spinal cord of patients with early cervical spondylotic myelopathy. Clinical Neurology and Neurosurgery. https://doi.org/10.1016/j.clineuro.2017.03.015

Li, D.-W., Wang, X.-M., 2015. Progresses of diffusion kurtosis imaging in spinal cord injury 31, 1422–1425. https://doi.org/10.13929/j.1003-3289.2015.09.036

Ljungberg, E., Vavasour, I., Tam, R., Yoo, Y., Rauscher, A., Li, D.K.B., Traboulsee, A., MacKay, A., Kolind, S., 2017. Rapid myelin water imaging in human cervical spinal cord. Magnetic Resonance in Medicine. https://doi.org/10.1002/mrm.26551

Loucao, R., Nunes, R.G., Neto-Henriques, R., Correia, M., Ferreira, H., 2015. Human brain tractography: A DTI vs DKI comparison analysis. https://doi.org/10.1109/enbeng.2015.7088820

Mader, I., Urbach, H., 2013. Walk the line: From diffusion imaging to the microstructure of the brain. Clinical Neuroradiology. https://doi.org/10.1007/s00062-013-0265-3

Martin, A.R., de Leener, B., Cohen-Adad, J., Cadotte, D.W., Kalsi-Ryan, S., Lange, S.F., Tetreault, L., Nouri, A., Crawley, A., Mikulis, D.J., Ginsberg, H., Fehlings, M.G., 2017. A novel MRI biomarker of spinal cord white matter injury: T2∗-weighted white matter to gray matter signal intensity ratio. American Journal of Neuroradiology. https://doi.org/10.3174/ajnr.A5162

Massire, A., Taso, M., Besson, P., Guye, M., Ranjeva, J.P., Callot, V., 2016. High-resolution multi-parametric quantitative magnetic resonance imaging of the human cervical spinal cord at 7T. NeuroImage. https://doi.org/10.1016/j.neuroimage.2016.08.055

McCoy, D.B., Talbott, J.F., Wilson, Michael, Mamlouk, M.D., Cohen-Adad, J., Wilson, Mark, Narvid, J., 2017. MRI atlas-based measurement of spinal cord injury predicts outcome in acute flaccid myelitis. American Journal of Neuroradiology. https://doi.org/10.3174/ajnr.A5044

Mohamed, F.B., Hunter, L.N., Barakat, N., Liu, C.S.J., Sair, H., Samdani, A.F., Betz, R.R., Faro, S.H., Gaughan, J., Mulcahey, M.J., 2011. Diffusion tensor imaging of the pediatric spinal cord at 1.5T: Preliminary results. American Journal of Neuroradiology. https://doi.org/10.3174/ajnr.A2334

Mulcahey, M.J., Samdani, A.F., Gaughan, J.P., Barakat, N., Faro, S., Shah, P., Betz, R.R., Mohamed, F.B., 2013. Diagnostic accuracy of diffusion tensor imaging for pediatric cervical spinal cord injury. Spinal Cord. https://doi.org/10.1038/sc.2013.36

Neto Henriques, R., 2012. Diffusion kurtosis imaging of the healthy human brain 134.

Oskouian, R.J., Sansur, C.A., Shaffrey, C.I., 2007. Congenital Abnormalities of the Thoracic and Lumbar Spine. Neurosurgery Clinics of North America. https://doi.org/10.1016/j.nec.2007.04.004

Panara, V., Navarra, R., Mattei, P.A., Piccirilli, E., Bartoletti, V., Uncini, A., Caulo, M., 2019. Correlations between cervical spinal cord magnetic resonance diffusion tensor and diffusion kurtosis imaging metrics and motor performance in patients with chronic ischemic brain lesions of the corticospinal tract. Neuroradiology. https://doi.org/10.1007/s00234-018-2139-5

Panara, V., Navarra, R., Mattei, P.A., Piccirilli, E., Cotroneo, A.R., Papinutto, N., Henry, R.G., Uncini, A., Caulo, M., 2017. Spinal cord microstructure integrating phase-sensitive inversion recovery and diffusional kurtosis imaging. Neuroradiology. https://doi.org/10.1007/s00234-017-1864-5

Paydar, A., Fieremans, E., Nwankwo, J.I., Lazar, M., Sheth, H.D., Adisetiyo, V., Helpern, J.A., Jensen, J.H., Milla, S.S., 2014. Diffusional kurtosis imaging of the developing brain. American Journal of Neuroradiology. https://doi.org/10.3174/ajnr.A3764

Pierpaoli, C., Basser, P.J., 1996. Toward a quantitative assessment of diffusion anisotropy. Magnetic Resonance in Medicine. https://doi.org/10.1002/mrm.1910360612

Pierpaoli, C., Jezzard, P., Basser, P.J., Barnett, A., di Chiro, G., 1996. Diffusion tensor MR imaging of the human brain. Radiology. https://doi.org/10.1148/radiology.201.3.8939209

Raz, E., Bester, M., Sigmund, E.E., Tabesh, A., Babb, J.S., Jaggi, H., Helpern, J., Mitnick, R.J., Inglese, M., 2013. A better characterization of spinal cord damage in multiple sclerosis: A diffusional kurtosis imaging study, in: American Journal of Neuroradiology. https://doi.org/10.3174/ajnr.A3512

Reynolds, B.B., By, S., Weinberg, Q.R., Witt, A.A., Newton, A.T., Feiler, H.R., Ramkorun, B., Clayton, D.B., Couture, P., Martus, J.E., Adams, M., Wellons, J.C., Smith, S.A., Bhatia, A., 2019. Quantification of DTI in the pediatric spinal cord: Application to clinical evaluation in a healthy patient population. American Journal of Neuroradiology. https://doi.org/10.3174/ajnr.A6104

Rufener, S., Ibrahim, M., Parmar, H.A., 2011. Imaging of Congenital Spine and Spinal Cord Malformations. Neuroimaging Clinics of North America. https://doi.org/10.1016/j.nic.2011.05.011

S Basu, P., Elsebaie, H., Noordeen, M., 2002. Congenital spinal deformity: A comprehensive assessment at presentation. Spine. https://doi.org/10.1097/00007632-200210150-00014

Saksena, S., Alizadeh, M., Middleton, D.M., Conklin, C.J., Krisa, L., Flanders, A., Mulcahey, M., Mohamed, F.B., Faro, S.H., 2018a. Characterization of spinal cord diffusion tensor imaging metrics in clinically asymptomatic pediatric subjects with incidental congenital lesions. Spinal Cord Series and Cases. https://doi.org/10.1038/s41394-018-0073-8

Saksena, S., Middleton, D.M., Krisa, L., Shah, P., Faro, S.H., Sinko, R., Gaughan, J., Finsterbusch, J., Mulcahey, M.J., Mohamed, F.B., 2016. Diffusion tensor imaging of the normal cervical and thoracic pediatric spinal cord. American Journal of Neuroradiology. https://doi.org/10.3174/ajnr.A4883

Saksena, S., Mohamed, F.B., Middleton, D.M., Krisa, L., Alizadeh, M., Shahrampour, S., Conklin, C.J., Flanders, A., Finsterbusch, J., Mulcahey, M.J., Faro, S.H., 2018b. Diffusion Tensor Imaging Assessment of Regional White Matter Changes in the Cervical and Thoracic Spinal Cord in Pediatric Subjects. Journal of Neurotrauma 36, 853–861. https://doi.org/10.1089/neu.2018.5826

Samson, R.S., Lévy, S., Schneider, T., Smith, A.K., Smith, S.A., Cohen-Adad, J., Wheeler-Kingshott, C.A.M.G., 2016. ZOOM or Non-ZOOM? Assessing spinal cord diffusion tensor imaging protocols for multi-centre studies. PLoS ONE. https://doi.org/10.1371/journal.pone.0155557

Singh, G., True, A.J., Lui, C.C., Prasanna, P., Orleans, G., Partyka, L., Phatak, T.D., 2020. Normal anterior-posterior diameters of the spinal cord and spinal canal in healthy term newborns on sonography. Pediatric Radiology. https://doi.org/10.1007/s00247-020-04879-8

Singhi, S., Tekes, A., Thurnher, M., Gilson, W.D., Izbudak, I., Thompson, C.B., Huisman, T.A.G.M., 2012. Diffusion tensor imaging of the maturing paediatric cervical spinal cord: From the neonate to the young adult. Journal of Neuroradiology. https://doi.org/10.1016/j.neurad.2011.05.002

Smith, A.C., Weber, K.A., O'Dell, D.R., Parrish, T.B., Wasielewski, M., Elliott, J.M., 2018. Lateral Corticospinal Tract Damage Correlates With Motor Output in Incomplete Spinal Cord Injury. Archives of Physical Medicine and Rehabilitation. https://doi.org/10.1016/j.apmr.2017.10.002

Sorantin, E., Robl, T., Lindbichler, F., Riccabona, M., 2008. MRI of the neonatal and paediatric spine and spinal canal. European Journal of Radiology. https://doi.org/10.1016/j.ejrad.2008.06.032

Steven, A.J., Zhuo, J., Melhem, E.R., 2014. Diffusion kurtosis imaging: An emerging technique for evaluating the microstructural environment of the brain. American Journal of Roentgenology. https://doi.org/10.2214/AJR.13.11365

Taber, K.H., Herrick, R.C., Weathers, S.W., Kumar, A., Schomer, D.F., Hayman, L.A., 1998. Pitfalls and Encountered Clinical Artifacts in Imaging of the Spine1. Radiographics : a review publication of the Radiological Society of North America, Inc.

Talbott, J.F., Narvid, J., Chazen, J.L., Chin, C.T., Shah, V., 2016. An Imaging-Based Approach to Spinal Cord Infection. Seminars in Ultrasound, CT and MRI. https://doi.org/10.1053/j.sult.2016.05.006

Taso, M., Girard, O.M., Duhamel, G., le Troter, A., Feiweier, T., Guye, M., Ranjeva, J.P., Callot, V., 2016. Tract-specific and age-related variations of the spinal cord microstructure: A multi-parametric MRI study using diffusion tensor imaging (DTI) and inhomogeneous magnetization transfer (ihMT). NMR in Biomedicine. https://doi.org/10.1002/nbm.3530

Tax, C.M.W., Otte, W.M., Viergever, M.A., Dijkhuizen, R.M., Leemans, A., 2015. REKINDLE: Robust Extraction of Kurtosis INDices with Linear Estimation. Magnetic Resonance in Medicine. https://doi.org/10.1002/mrm.25165

Thukral, B.B., 2015. Problems and preferences in pediatric imaging. Indian Journal of Radiology and Imaging. https://doi.org/10.4103/0971-3026.169466

Toselli, B., Tortora, D., Severino, M., Arnulfo, G., Canessa, A., Morana, G., Rossi, A., Fato, M.M., 2017. Improvement in white matter tract reconstruction with constrained spherical deconvolution and track density mapping in low angular resolution data: A pediatric study and literature review. Frontiers in Pediatrics. https://doi.org/10.3389/fped.2017.00182

Tournier, J.D., 2019. Diffusion MRI in the brain – Theory and concepts. Progress in Nuclear Magnetic Resonance Spectroscopy. https://doi.org/10.1016/j.pnmrs.2019.03.001

Tournier, J.D., Smith, R., Raffelt, D., Tabbara, R., Dhollander, T., Pietsch, M., Christiaens, D., Jeurissen, B., Yeh, C.H., Connelly, A., 2019. MRtrix3: A fast, flexible and open software framework for medical image processing and visualisation. NeuroImage. https://doi.org/10.1016/j.neuroimage.2019.116137

Tustison, N.J., Avants, B.B., 2013. Explicit B-spline regularization in diffeomorphic image registration. Frontiers in Neuroinformatics. https://doi.org/10.3389/fninf.2013.00039

Ullmann, E., Pelletier Paquette, J.F., Thong, W.E., Cohen-Adad, J., 2014. Automatic Labeling of Vertebral Levels Using a Robust Template-Based Approach. International Journal of Biomedical Imaging. https://doi.org/10.1155/2014/719520

Vahdat, S., Lungu, O., Cohen-Adad, J., Marchand-Pauvert, V., Benali, H., Doyon, J., 2015. Simultaneous brain–cervical cord fMRI reveals intrinsic spinal cord plasticity during motor sequence learning. PLoS Biology. https://doi.org/10.1371/journal.pbio.1002186

Ventura, R.E., Kister, I., Chung, S., Babb, J.S., Shepherd, T.M., 2016. Cervical spinal cord atrophy in nmosd without a history of myelitis or MRI-visible lesions. Neurology: Neuroimmunology and NeuroInflammation. https://doi.org/10.1212/NXI.0000000000000224

Veraart, J., Poot, D.H.J., van Hecke, W., Blockx, I., van der Linden, A., Verhoye, M., Sijbers, J., 2011. More accurate estimation of diffusion tensor parameters using diffusion Kurtosis imaging. Magnetic resonance in medicine : official journal of the Society of Magnetic Resonance in Medicine / Society of Magnetic Resonance in Medicine. https://doi.org/10.1002/mrm.22603

Volpe, J.J., Inder, T.E., Darras, B.T., de Vries, L.S., du Plessis, A.J., Neil, J.J., Perlman, J., 2017. Volpe's neurology of the newborn, Volpe's Neurology of the Newborn. https://doi.org/10.1016/c2010-0-68825-0

Weber, K.A., Chen, Y., Wang, X., Kahnt, T., Parrish, T.B., 2016. Lateralization of cervical spinal cord activity during an isometric upper extremity motor task with functional magnetic resonance imaging. NeuroImage. https://doi.org/10.1016/j.neuroimage.2015.10.014

Weber, K.A., Sentis, A.I., Bernadel-Huey, O.N., Chen, Y., Wang, X., Parrish, T.B., Mackey, S., 2018. Thermal Stimulation Alters Cervical Spinal Cord Functional Connectivity in Humans. Neuroscience. https://doi.org/10.1016/j.neuroscience.2017.10.035

Webster, J.G., Descoteaux, M., 2015. High Angular Resolution Diffusion Imaging (HARDI), in: Wiley Encyclopedia of Electrical and Electronics Engineering. https://doi.org/10.1002/047134608x.w8258

Wilm, B.J., Svensson, J., Henning, A., Pruessmann, K.P., Boesiger, P., Kollias, S.S., 2007. Reduced field-of-view MRI using outer volume suppression for spinal cord diffusion imaging. Magnetic Resonance in Medicine. https://doi.org/10.1002/mrm.21167

Wu, E.X., Cheung, M.M., 2010. MR diffusion kurtosis imaging for neural tissue characterization. NMR in Biomedicine. https://doi.org/10.1002/nbm.1506

Xu, J., Shimony, J.S., Klawiter, E.C., Snyder, A.Z., Trinkaus, K., Naismith, R.T., Benzinger, T.L.S., Cross, A.H., Song, S.K., 2013. Improved in vivo diffusion tensor imaging of human cervical spinal cord. NeuroImage. https://doi.org/10.1016/j.neuroimage.2012.11.014

Yang, R.K., Roth, C.G., Ward, R.J., deJesus, J.O., Mitchell, D.G., 2010. Optimizing abdominal MR imaging: Approaches to common problems. Radiographics. https://doi.org/10.1148/rg.301095076

Yiannakas, M.C., Mustafa, A.M., de Leener, B., Kearney, H., Tur, C., Altmann, D.R., de Angelis, F., Plantone, D., Ciccarelli, O., Miller, D.H., Cohen-Adad, J., Gandini Wheeler-Kingshott, C.A.M., 2016. Fully automated segmentation of the cervical cord from T1-weighted MRI using PropSeg: Application to multiple sclerosis. NeuroImage: Clinical. https://doi.org/10.1016/j.nicl.2015.11.001

Zhang, H., Schneider, T., Wheeler-Kingshott, C.A., Alexander, D.C., 2012. NODDI: Practical in vivo neurite orientation dispersion and density imaging of the human brain. NeuroImage. https://doi.org/10.1016/j.neuroimage.2012.03.072